



## VULNERABILITY ASSESSMENT OF HISTORIC STRUCTURES IN KATHMANDU, NEPAL

J. Kiyono<sup>(1)</sup>, A. Furukawa<sup>(2)</sup>, H. R. Parajuli<sup>(3)</sup>, P. N. Maskey<sup>(4)</sup> and R. R. Parajuli<sup>(5)</sup>

<sup>(1)</sup> Professor, Graduate School of Global Environmental Studies, Kyoto University, kiyono.junji.5x@kyoto-u.ac.jp

<sup>(2)</sup> Associate Professor, Graduate School of Global Environmental Studies, Kyoto University, furukawa.aiko.3w@kyoto-u.ac.jp

<sup>(3)</sup> Lecturer, Institute of Engineering, Tribhuvan University, hariparajuli@ioe.edu.np

<sup>(4)</sup> Professor, Institute of Engineering, Tribhuvan University, pnmaskey@live.com

<sup>(5)</sup> Doctoral student, Graduate School of Engineering, Kyoto University, parajuli.ram.27z@st.kyoto-u.ac.jp

### **Abstract**

Nepal is located on a part of the Himalayan orogeny that has induced many destructive earthquakes there and in surrounding areas. Kathmandu is the capital and a center of culture in Nepal. Unfortunately, many historic buildings have been damaged by earthquakes over the centuries because of its location in an earthquake-prone area. In particular, an earthquake impacting Kathmandu in 1934 had a magnitude greater than 8, destroying most of the cultural heritage sites, such as temples, shrines and monuments. Recently, Nepal suffered catastrophic damage caused by a destructive earthquake on April 25, 2015. The first priority in such events is to save as many human lives as possible and protect people from secondary disaster. However, historic structures in world heritage sites can never be replaced, because of their authentic character. To solve this major problem, detailed investigation of such historic structures is indispensable. The ultimate goal is to formulate comprehensive risk mitigation planning strategies for historic areas in Kathmandu. We selected for study a historical masonry building in the Jhatapol area, near Patani Durbar Square. This building was constructed in the 18th century and is currently used as an assembly house. With the aim of developing strengthening techniques for heritage buildings and as a first step toward seismic disaster risk mitigation, the structure of the building was analyzed using the refined distinct element method (RDEM). In this study, the strength of materials of the building was investigated through experiments. Following that investigation and determination of other structural parameters, a numerical model of the building was verified by observation of dominant frequencies. Seismic vulnerability of historic buildings was examined. After verifying that the natural frequencies from the analytical model coincided with those from microtremor observations, seismic behaviors of the targeted masonry building were analyzed using RDEM. When ground motions with occurrence probabilities of 10% and 5% over 50 years were input, there was more severe damage, especially when those motions were in a direction transverse to the building.

*Keywords: historic structure; vulnerability assessment; brick masonry structure; experiment of masonry wall; RDEM*



## 1. Introduction

Nepal is located on a part of the Himalayan orogeny that has induced many destructive earthquakes there and in surrounding areas. Kathmandu is the capital and a center of culture in Nepal. Unfortunately, many historic buildings have been damaged by earthquakes over the centuries, because of its location in an earthquake-prone area. In particular, an earthquake that struck Kathmandu in 1934 had a magnitude greater than 8, destroying most of the cultural heritage, such as temples, shrines and monuments [1].

UNESCO designated seven sites in the Kathmandu Valley as World Heritage sites in 1979. However, many historic masonries with tiled roofs and composite buildings of masonry and timber were demolished because of industrialization and commercialization. This was followed by increasing concrete building construction with low quality. Therefore, the Kathmandu Valley was registered in the List of World Heritage in Danger in 2003. Afterward, owing to valiant efforts by the World Heritage Committee and associated ministries of Nepal, the valley was unlisted in 2007 [2]. Many efforts have been made for the protection of cultural heritage; however, efforts to protect it from earthquake disasters have been inadequate. A recent destructive earthquake, in which many heritage structures collapsed or were severely damaged, proved this assertion. Damaged historic monuments, temples and shrines have been demolished or reconstructed as reinforced concrete buildings of no historic value [2].

In 2002, seismic damage to buildings in Kathmandu was estimated by the Japanese government (through JICA) using a simple method with a structural vulnerability function [3]. This was a useful technical support for protecting historic structures from earthquake disaster. However, because the vulnerability function was statistically constructed from past earthquake data worldwide, it did not provide a Kathmandu-specific vulnerability assessment. Moreover, because the vulnerability function was mainly based on damaged residential buildings, it is not necessarily suitable for historic buildings. Therefore, seismic resistance of existing historic buildings in Nepal remains unclear.

In this study, we investigate seismic vulnerability of an existing historic masonry building in the Jhatapo area. Numerical simulations by the refined distinct element method (RDEM) developed by the authors [4] were used, based on parameters obtained from structural element experiments. Results were obtained for three input ground motions with different occurrence probabilities, and two cases with different input ground motion directions were compared.

## 2. Method of Numerical Analysis

### 2.1 Basic concept

We used a refined version of the DEM [4] to simulate a series of structural dynamic behaviors, from elastic to failure to collapse phenomena. The program was developed by the authors and written in Fortran language. A structure is modeled as an assembly of rigid elements, and interaction between those elements is modeled by multiple springs and dashpots that are attached to element surfaces. The elements are rigid, but the method allows simulation of structural deformation by permitting penetration between elements.

Figure 1a shows a spring for computing the restoring force (restoring spring), which models the elasticity of elements. For simplicity in the figure, a shear spring is set in one direction, but actually has two directions. The restoring spring is set between continuous elements. Structural failure is modeled as breakage of the restoring spring, at which time the restoring spring is replaced by a contact spring and contact dashpot (Fig. 1b). The latter figure shows the spring and dashpot for computing the contact force (contact spring and dashpot) and modeling the contact, separation, and re-contact between elements. The dashpots are introduced to express energy dissipation by the contact. Structural collapse behavior is determined using these springs and dashpots. The elements shown in Fig. 1a and b are rectangular parallelepipeds, but the method does not limit the element geometry.

The surface of an element is divided into small segments, as shown in Fig. 1c. The segment in the figure is rectangular, but the method does not limit segment geometry. Black points indicate points representative of each segment, and relative or contact displacements between elements are computed for these points. Such points are referred to as contact or master points in this study. One restoring spring and one combination of contact spring and dashpot were attached to one segment (Fig. 1d) at each of the representative points in Fig. 1c. The spring

constant for each segment was derived on the basis of the stress-strain relationship of the material and segment area.

Forces acting on each element were obtained by summing the restoring force, contact force, and other external forces such as the gravitational and inertial forces of an earthquake. The behavior of an element consists of the translational behavior of the center of gravity and rotational behavior around that center. The translational and rotational behaviors of each element are computed explicitly by solving Newton's law of motion and Euler's equation of motion.

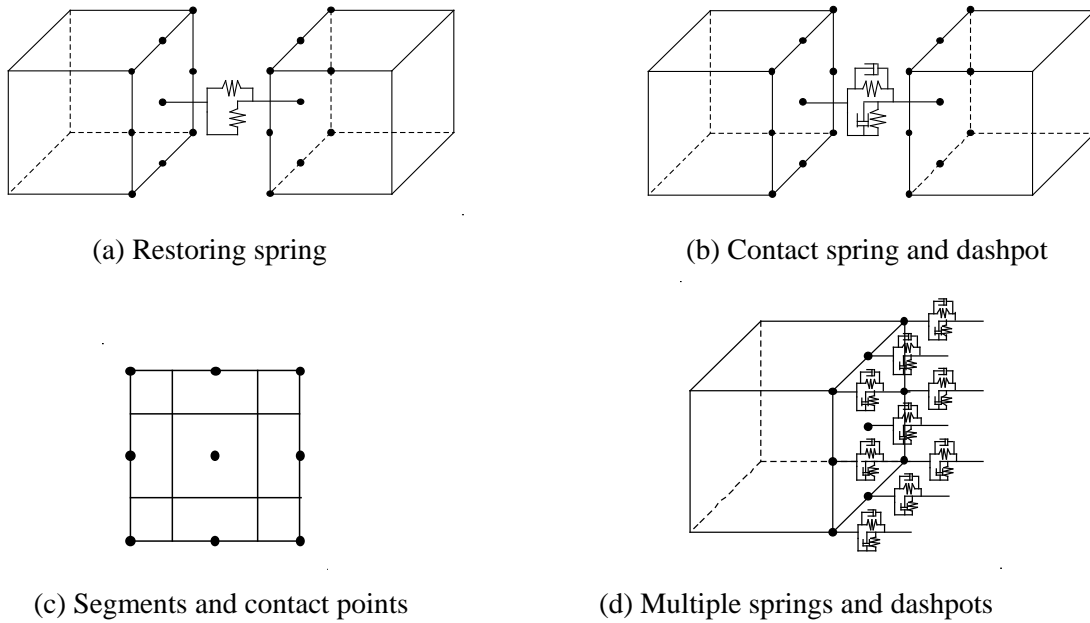


Fig. 1 – Basic concept of analysis method [4]

## 2.2 Spring constant of each element

There are two types of springs, restoring and contact. It was assumed that the spring constants of the restoring and contact springs are identical, and that each segment has its own spring.

Springs were set for both the normal and shear (tangential) directions of the surface. Let us denote the area of the segment as  $dA$  and relative (contact) displacement at the surface segment as  $u_n$  and  $u_s$ , where subscripts  $n$  and  $s$  indicate values in the normal and shear directions, respectively. The spring constants per area in the normal and shear directions,  $k_n$  and  $k_s$ , are obtained as follows.

$$k_n = \frac{E}{(1-\nu^2)\ell} \quad k_s = \frac{E}{2(1+\nu)\ell} \quad (1)$$

where  $E$  is Young's modulus,  $\nu$  is Poisson's ratio, and  $\ell$  is the distance from the surface at which the spring is connected to the center of gravity. In masonry structures, bricks are often connected with mortar. In this case, the spring constant per area between elements (bricks) is obtained as

$$\bar{k}_n = \frac{1}{\frac{\ell_A - t_M / 2}{E_A / (1-\nu_A^2)} + \frac{t_M}{E_M / (1-\nu_M^2)} + \frac{\ell_B - t_M / 2}{E_B / (1-\nu_B^2)}} \quad \bar{k}_s = \frac{1}{\frac{\ell_A - t_M / 2}{E_A / 2(1+\nu_A)} + \frac{t_M}{E_M / 2(1+\nu_M)} + \frac{\ell_B - t_M / 2}{E_B / 2(1+\nu_B)}} \quad (2)$$

where  $t_M$  is mortar thickness,  $E_M$  is Young's modulus, and  $\nu_M$  is Poisson's ratio of the mortar. The normal direction of forces is perpendicular to the surface of the master point of element A.



### 2.3 Modeling of failure phenomena

The elastic behavior of structures was demonstrated by the linear multiple restoring springs between continuous elements until the restoring force of a spring reached its elastic limit. The elastic limits were modeled using the criteria of tension, shear, and compression failure. When a spring reached one of these limits, we determined that failure had occurred at that segment of the spring. After this failure, the restoring spring at the segment was replaced with a contact spring and dashpot. This method can trace the expansion of failure between elements. The three failure modes—tension, shear, and compression—were defined based on the Mohr-Coulomb cap model.

### 2.4 Equations of motion

Equations of motion can be constructed using the restoring and contact forces and other external forces. The motion of each element is obtained by solving the two equations of motion. One is the equation for the translational motion of the center of gravity, and the other is the equation for rotational motion around that center.

$$m\ddot{\mathbf{x}}_g(t) + c\dot{\mathbf{x}}_g(t) = m\mathbf{g} - m\ddot{\mathbf{z}}(t) + \sum \mathbf{F}(t) \quad (3)$$

$$\mathbf{I}\dot{\boldsymbol{\omega}}(t) + \boldsymbol{\omega}(t) \times \mathbf{I}\boldsymbol{\omega}(t) = \sum \mathbf{R}(t)\mathbf{r}(t) \times \mathbf{R}(t)\mathbf{F}(t), \quad (4)$$

where  $\mathbf{x}_g(t)$  is the displacement vector of the center of gravity of an element at time  $t$ ,  $m$  is mass of the element,  $c$  is the damping constant of the element,  $\mathbf{g}$  is the gravitational acceleration vector,  $\ddot{\mathbf{z}}_i$  is the ground acceleration vector at  $t$ ,  $\sum \mathbf{F}(t)$  is the sum of the restoring and contact force vectors at  $t$ ,  $\mathbf{I}$  is the tensor of the moment of inertia, and  $\mathbf{r}(t)$  is the vector between the center of gravity and the point where force  $\mathbf{F}(t)$  is applied.  $\mathbf{R}(t)$  is the matrix representing the transformation from the absolute coordinate system to inertial frame of reference.

## 3. Target Structure and Analytical Model

### 3.1 Target historic masonry building

The building analyzed is a historic composite building whose location and photos are shown in Figs. 2 and 3. It was built in the 17th century. It has been damaged by several earthquakes and repaired many times.

The building is two-storied and has dimensions 16.5 m  $\times$  5.6 m. Heights of the 1st and 2nd floors are 2.4 and 2.1 m, respectively. The maximum building height is 6.5 m. Each wall has openings, with the western wall having the largest (Fig. 3a). The walls are composed of bricks, which are connected with each other by mortar. The brick size is not uniform, and depends on when and where they were made. There are two separate rooms of width 2–3 m (Fig. 3c).

### 3.2 Analytical model

The analytical model is shown in Fig. 4a, b and c. Members except bricks, such as columns, beams and ring beams, are shown in Fig. 4d. The coordinate axis is shown in Fig. 4a. In the western wall, there are eight wooden vertical columns on the 1st floor, and six wooden vertical columns and two wooden horizontal beams on the 2nd floor. There are two ring beams atop both floors. The depth of the walls is 55 cm.

Table 1 lists material properties such as mass density, Young's modulus and Poisson's ratio, tensile strength, bonding strength, friction angle, and compressive strength. Values used for bricks are not actual values of a single brick, but average ones of the wall including bricks and mortar. Properties were estimated through an experiment using bricks taken from an existing building [5, 6]. Because material properties of wooden columns and beams on the western wall were not measured, general values for woods were used instead [7]. The roof is made of tin and was not modeled, considering that its weight is very light and does not affect vibration behavior.



Fig. 2 – Target (Jhatapo) area and location of target building



(a) Western wall



(b) Eastern wall



(c) Eastern room of 2nd floor

Fig. 3 – Target historic masonry building

Table 1 – Parameters used in analysis

Variable	Adobe Brick	Mortar	Wood
Mass density ( $\text{kg/m}^3$ )	$1.8 \times 10^3$	-	$7.0 \times 10^2$
Young's modulus ( $\text{N/m}^2$ )	$2.7 \times 10^8$	$2.7 \times 10^8$	$6.3 \times 10^8$
Poisson's ratio	0.11	0.25	0.3
Tensile strength $f_t$ ( $\text{N/m}^2$ )	-	0.0	$1.1 \times 10^8$
Shear strength $c$ ( $\text{N/m}^2$ )	-	$9.0 \times 10^4$	$9.0 \times 10^6$
Friction angle $\phi$	-	$42.5^\circ$	$0^\circ$
Compressive strength ( $\text{N/m}^2$ )	-	$1.58 \times 10^6$	$4.5 \times 10^7$

The building was modeled as an assembly of rigid elements of rectangular parallelepipeds. The size of each brick was  $10 \text{ cm} \times 10 \text{ cm} \times 20 \text{ cm}$ . The total number of elements was 63,978. The rigid elements were connected with each other by springs. The rigid element itself does not deform, but the building as a whole shows deformation by overlapping of the rigid elements. When one of the tensile, shear and compression stresses acting at the spring exceeds its strength, the spring is cut and failure occurrence is expressed.

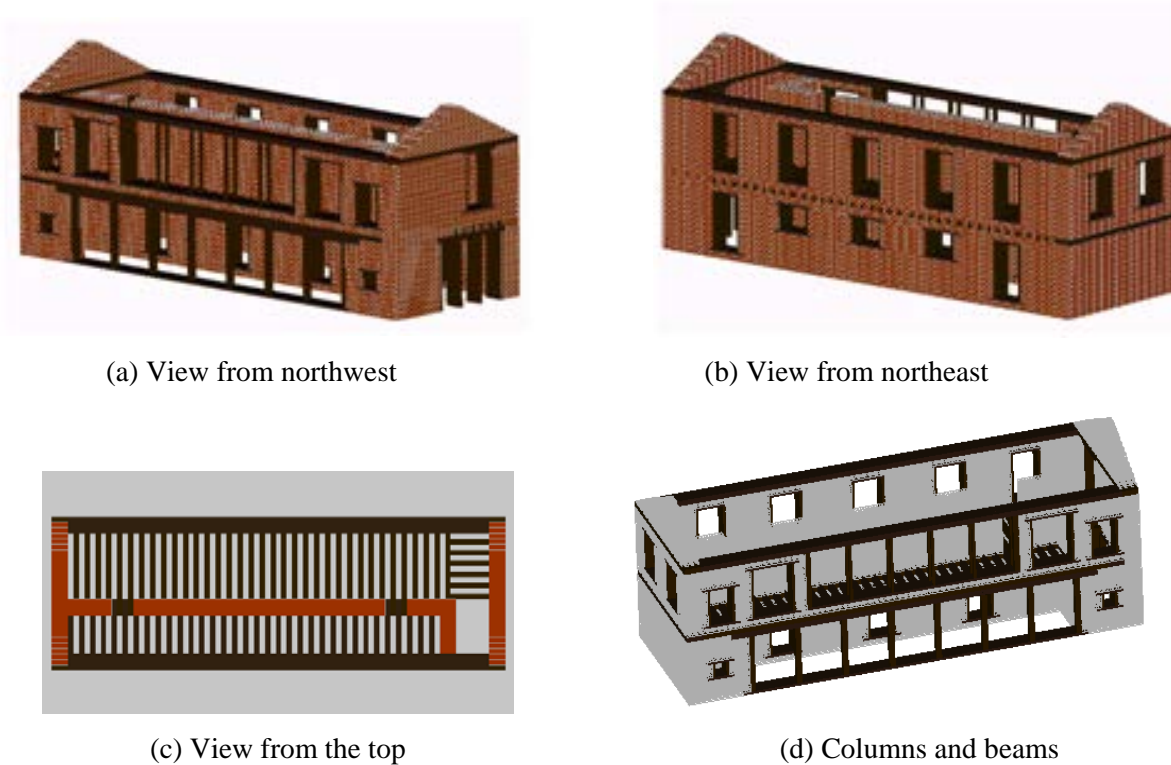


Fig. 4 – Analytical model

### 3.3 Verification of analytical model

The microtremors and natural frequencies were observed for the targeted building (Table 2). The first natural frequency was 4.3 Hz, which is a translational mode in the y direction. The second natural frequency was 5.8 Hz, a torsional mode. The third natural frequency was 6.8 Hz, a translational mode in the x direction.

To obtain the natural frequencies in the analytical model, an impact acceleration of 100 gal was input to the building in the x and y directions separately, and the displacement response was computed at one point on the 2nd floor. The displacement history in the x direction when the impact acceleration was input in the x direction is shown in Fig. 5a. The Fourier spectrum is shown in Fig. 5b. The displacement history in the y direction when the impact acceleration was input in the y direction is shown in Fig. 6a. The Fourier spectrum is shown in Fig. 6b. From these figures, the Fourier spectra for the y direction has a peak ~4.0 Hz, which corresponds to the translational mode in the y direction of the first mode. The Fourier spectra in both x and y directions have their peak ~5.0 Hz, which can be considered the torsional mode of the second mode. The Fourier spectrum for the x direction has a peak ~6.6 Hz, which can be considered the translational mode in the x direction of the third mode. From this comparison between analytical results and microtremor observation, the analytical model expressed the vibration characteristics almost correctly, so the validity of that model was confirmed.

Table 2 – Natural frequencies from microtremor observation

Mode number	1 <sup>st</sup> mode	2 <sup>nd</sup> mode	3 <sup>rd</sup> mode
Frequency	4.3Hz	5.8Hz	6.8Hz
Mode	Translational mode in Y direction	Torsional mode	Translational mode in X direction

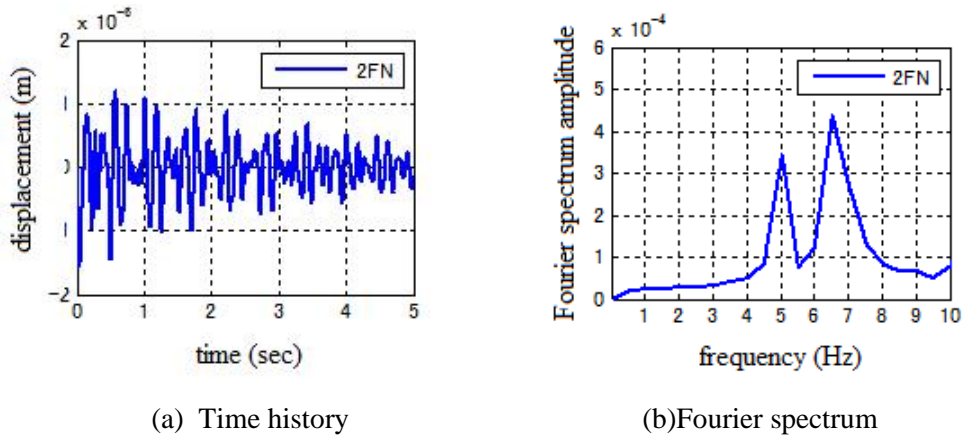


Fig. 5 – Displacement response in x direction when impact acceleration was input in x direction

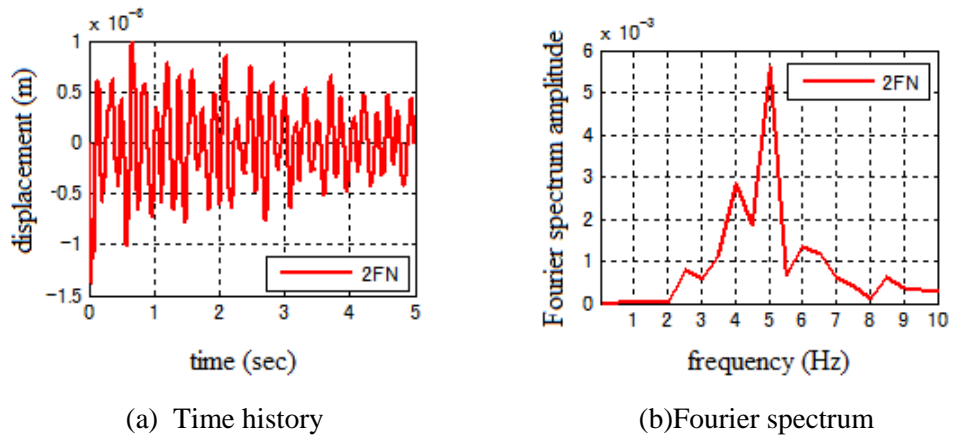


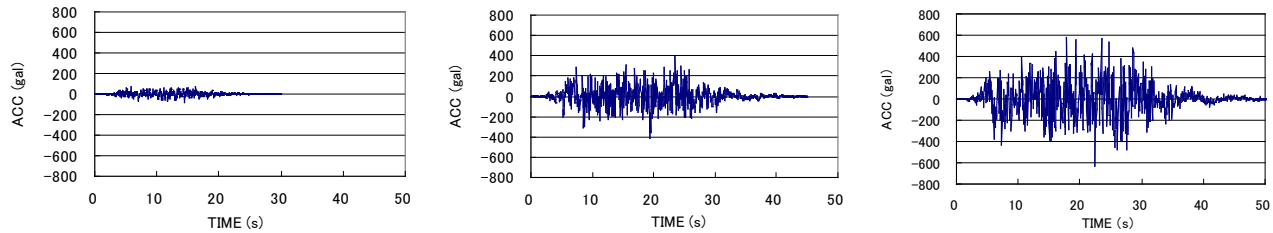
Fig.6 – Displacement response in y direction when impact acceleration was input in y direction

#### 4. Seismic Behavior of Historic Structure

Numerical simulations were conducted by changing input ground motion. Input ground accelerations are shown in Fig. 7. These were estimated from Nepalese historic seismic data and active fault data using seismic hazard analysis [8]. Figure 7a shows acceleration with occurrence probability of 40% within 50 years (return period is 98 years) and a maximum acceleration of 84 gal. Figure 7b shows acceleration with occurrence probability of 10% within 50 years (return period is 475 years) and a maximum acceleration of 420 gal. Figure 7c shows acceleration with occurrence probability of 5% within 50 years (return period is 975 years) and a maximum acceleration of 630 gal. The analytical cases are shown in Table 3. There were six cases, with two directions and three occurrence probabilities.

Table 3 – Cases with various directions and occurrence probabilities of input ground motion

Cases	Direction of input ground motion	Occurrence probability in 50 years
Case 1X	X	40%
Case 1Y	Y	40%
Case 2X	X	10%
Case 2Y	Y	10%
Case 3X	X	5%
Case 3Y	Y	5%



(a) 40% (return period 98 year) (b) 10% (return period 475 year) (c) 5% (return period 975 year)

Fig. 7 – Input ground acceleration with various occurrence probabilities (%) within 50 years [8]

#### 4.1 Input ground acceleration with occurrence probability of 40% within 50 years

The input ground motion with occurrence probability of 40% within 50 years was input in the x and y directions separately. Seismic behavior for these directions is shown in Figs. 8 and 9.

Looking at the triangle part on the shorter wall, the difference due to input ground motion directions cannot be seen. The northern wall completely collapsed and the southern wall partially collapsed. This is because the northern wall had larger openings on the second floor, which made that wall vibrate more.

When the input ground motion was input in the x direction (case 1X), more damage occurred to the wider wall compared to the case in which the input ground motion was input in the y direction (case 1Y). In case 1X, the northern part of the wall on the east side had severe damage. This is because ground motion in the x direction excited vibration of the shorter wall in the out-of-plane direction. The wall on the north side had larger openings on the 2nd floor, and was more likely to vibrate compared to the wall on the south side. Therefore, the upper part of the northern wall separated from the other part and collapsed, which caused failure of the eastern wall. The northern wall failed because of vibration in the out-of-plane direction, whereas the southern wall had slight damage. These observations show that the southern part with smaller openings on the 2nd floor had greater earthquake resistance than the northern wall. In case 1Y, both eastern and western walls were wide with larger openings, and vibrated readily in the out-of-plane direction. However, the western wall had less damage than the eastern wall. This is because columns in the western wall served as reinforcement and prevented its failure.

#### 4.2 Input ground acceleration with occurrence probability of 10% within 50 years

Ground motion with occurrence probability of 10% within 50 years was input in the x and y directions separately. Seismic behavior for these directions is shown in Figs. 10 and 11.

When the ground motion was input in the y direction, the building completely collapsed. The eastern wall first separated from the buildings and collapsed, then the shorter wall collapsed, and the western wall collapsed last. The reason why the western wall with the largest openings collapsed last is that the columns resisted tensile failure. When the ground motion was input in the x direction, both shorter walls were damaged on the 2nd floor, followed by failure of the 1st floor. This damaged southern parts of the eastern and western walls.

#### 4.3 Input ground acceleration with occurrence probability of 5% within 50 years

Finally, input ground motion with occurrence probability of 5% within 50 years was input in the x and y directions separately. Seismic behavior for these directions is shown in Figs. 12 and 13. Similar to the case with occurrence probability of 10%, the buildings collapsed when ground motion was input in the y direction. When that motion was input in the x direction, the 2nd floor collapsed but the 1st floor did not.

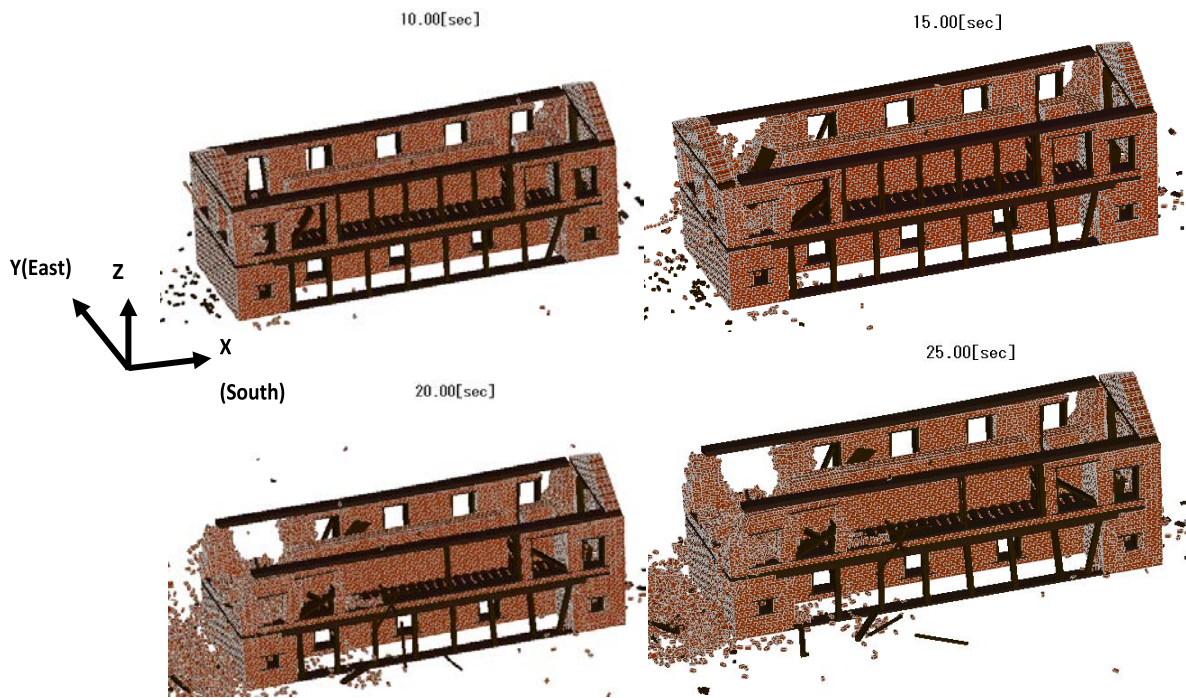


Fig. 8 – Seismic behavior in case 1X (ground motion input in x direction; 40% within 50 years)

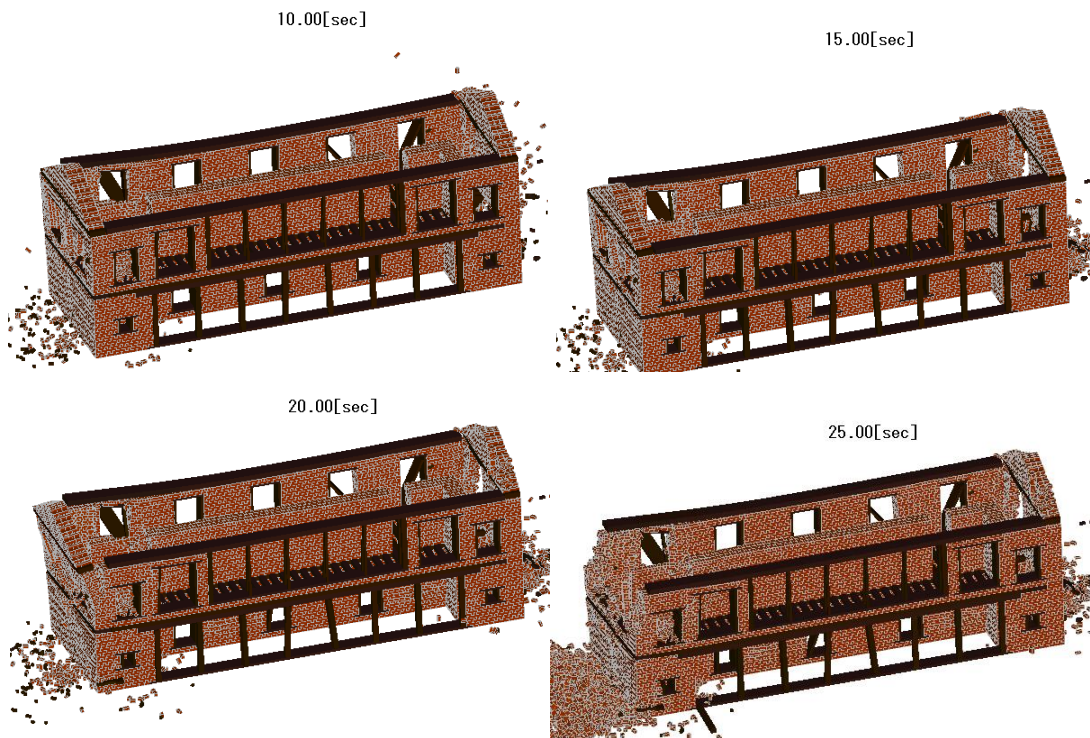


Fig. 9 – Seismic behavior in case 1Y (ground motion input in y direction; 40% within 50 years)

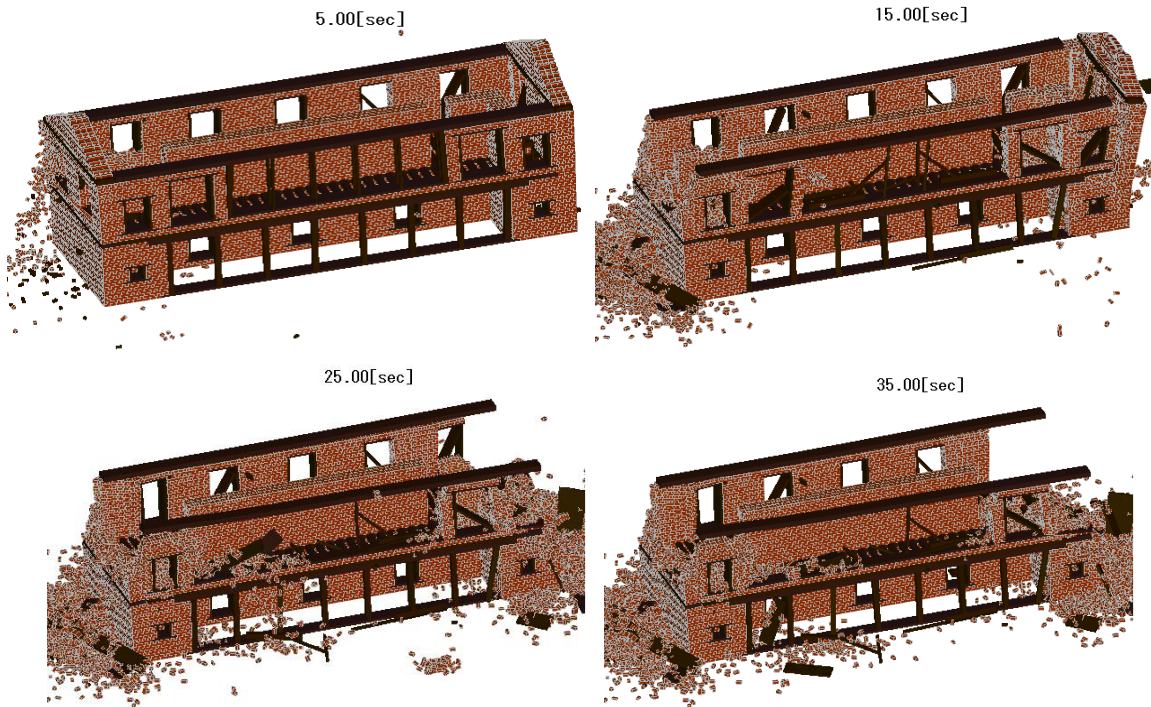


Fig. 10 – Seismic behavior in case 2X (ground motion input in x direction; 10% within 50 years)

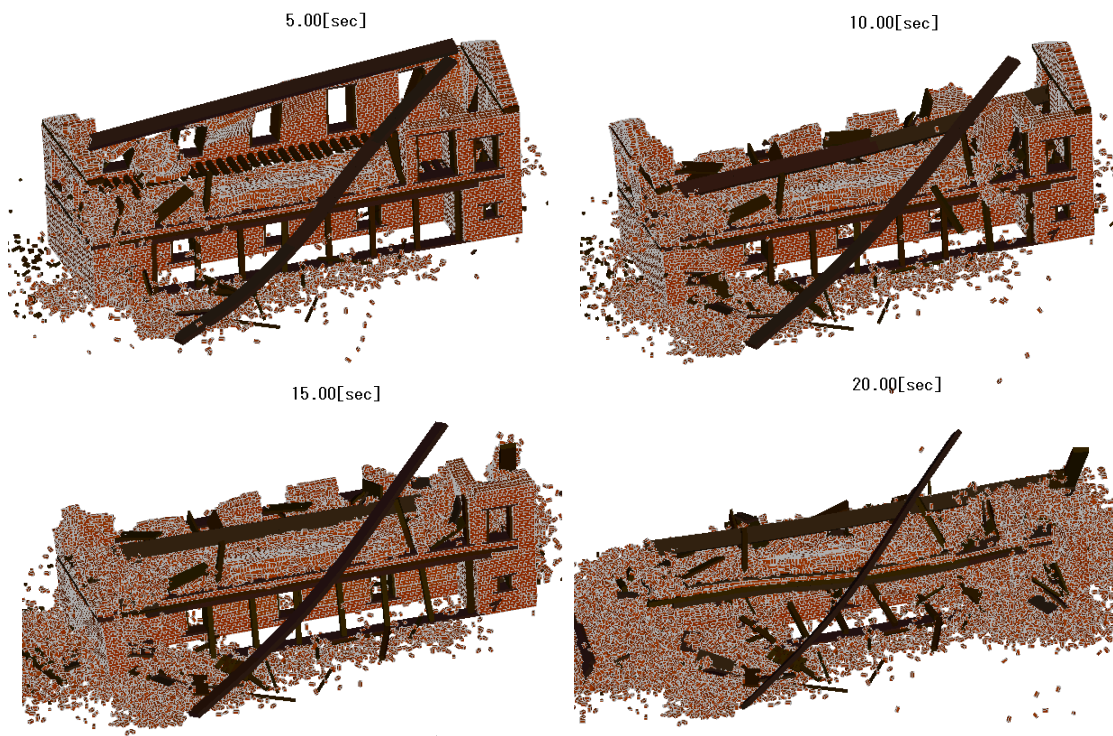


Fig. 11 – Seismic behavior in case 2Y (ground motion input in y direction; 10% within 50 years)

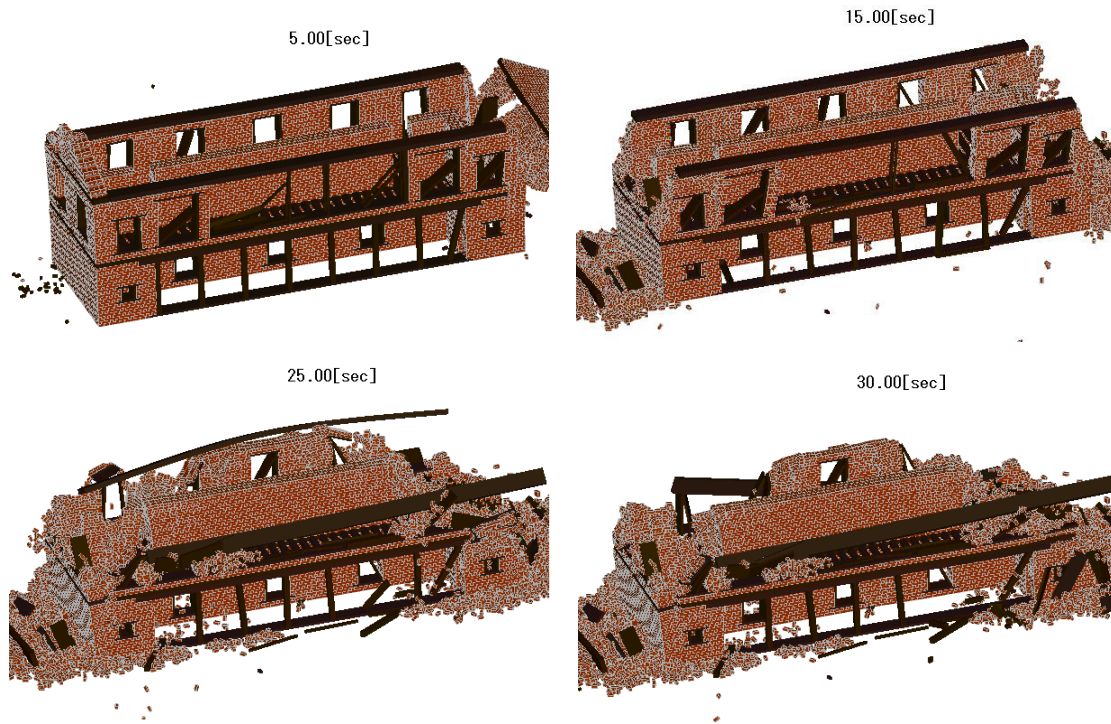


Fig. 12 – Seismic behavior in case 3X (ground motion input in x direction; 5% within 50 years)

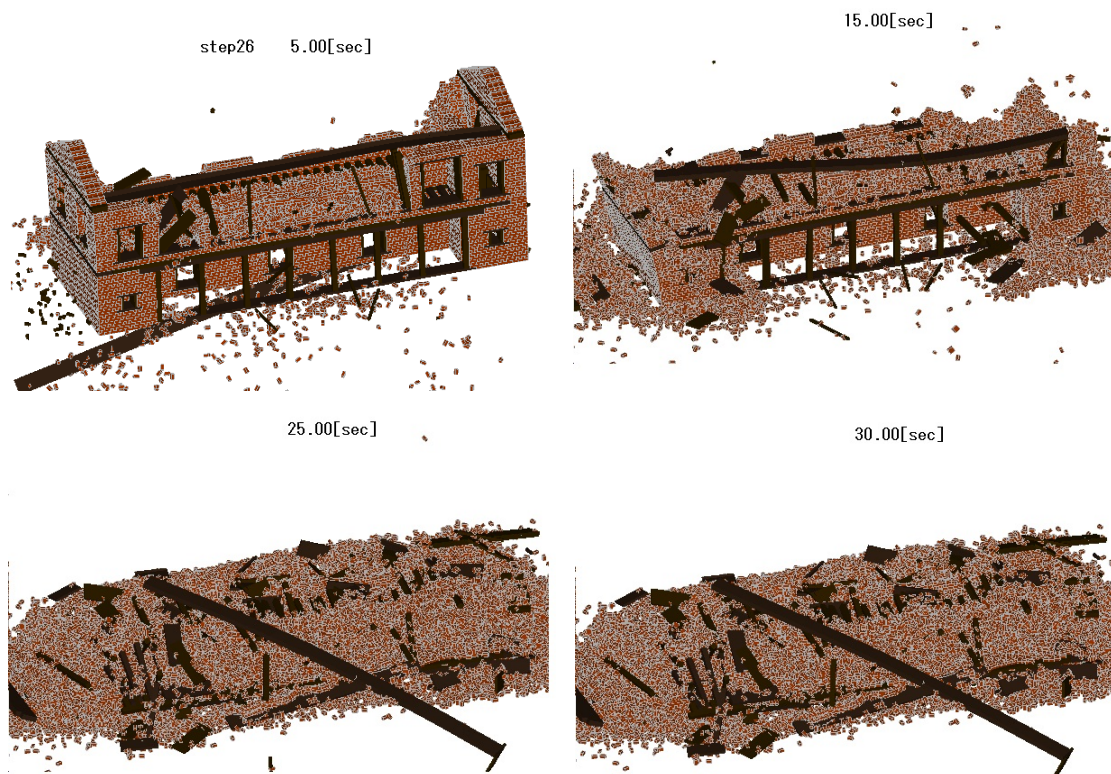


Fig. 13 – Seismic behavior in Case 3Y (ground motion input y direction; 5% within 50 years)



## 5. Discussion and Conclusions

Based on damage investigation surveys, typical failure patterns of adobe buildings have been addressed by many researchers [9, 10]. In the present work, the outcome of the DEM was compared with observed failure patterns to confirm the DEM performance. Mohmoud et al. [9] reported that out-of-plane failure of walls was the main failure mode of the adobe houses. They stated that lack of proper connections between perpendicular walls resulted in the separation of walls from each other, wall failure, and subsequent roof collapse. The DEM succeeded in demonstrating this failure mode. For example, in Fig. 9, out-of-plane deformation of the shorter walls on the south side is evident. Zahrai and Heidarzadeh [10] indicated that the failure of adobe buildings normally starts in a corner, through separation of the walls from the top. They found that separation between walls starts from the top. Our RDEM simulation demonstrates this behavior. Using our method, vulnerability of a target masonry structure can be assessed. This was a composite structure of masonry and wood. The mortar used was mad mortar. Most of the structures including monuments in a core zone of the heritage area have the same composite type and the mortar used between the bricks is mad mortar. We believe that the analysis and material parameters can be applied to the historic structures in the core zone.

We showed the procedure to assess vulnerability by analyzing seismic behavior of the existing masonry building, using the refined version of the DEM. The natural frequencies of the analytical model are in good agreement with those obtained from microtremor observations. When the ground motion with occurrence probabilities of 10% and 5% within 50 years is input, there was more severe damage, especially when the input was in the y direction.

## 6. Acknowledgments

This research was done under the support of the J-RAPID program of Japan Science and Technology Agency (JST), Japan Society for the Promotion of Science (JSPS) Grant-in-Aid (26249067), and Grant for Global Sustainability (GGS) initiated by the United Nations University (UNU). We express sincere appreciation to JST, JSPS and UNU.

## 7. References

- [1] Amatya, S (2008): *Monument conservation in Nepal*. Vajra Publications.
- [2] Rohit K.R.(2007): *Heritage homeowner's preservation handbook*. UNESCO.
- [3] JICA (2002): Final Report of JICA Study Team on Kathmandu Valley Earthquake Disaster Mitigation Planning.
- [4] Furukawa A, Kiyono J, Toki K (2001): Proposal of a numerical simulation method for elastic, failure and collapse behaviors of structures and its application to masonry walls, *Journal of Disaster Research*, **6** (1), Paper: Dr6-1-4524.
- [5] Kiyono J and Afshin Kalantari (2004): Collapse Mechanism of Adobe and Masonry Structures During the 2003 Iran Bam Earthquake, *Bull. Earthq. Res. Inst.*, Univ. Tokyo, **79**, 157-161.
- [6] Parajuli, Hari Ram, Junji Kiyono, Hitoshi Taniguchi (2010): Parametric study and dynamic analysis of a historical masonry building of Kathmandu, *Journal of Disaster Mitigation for Historical Cities*, **4**, 149-156.
- [7] Kiyono J and Furukawa A (2004): Casualty occurrence mechanism in the collapse of timber frame houses during an earthquake, *Earthquake Engineering & Structural Dynamics*, **33**, 1233-1248.
- [8] Parajuli HR, Kiyono J, Ono Y, and Tsutsumiuchi T (2007): Design earthquake ground motions from probabilistic response spectra: Case study of Nepal, *Journal of Japan Association for Earthquake Engineering*, **8** (4), 16-28.
- [9] Mahmoud RM, Farzad N, Michael M (2005): Performance of adobe residential buildings in the 2003 Bam, Iran, Earthquake, *Earthquake Spectra*, **21** (S1), S337-S344, 2005.
- [10] Zahrai SM, Heidarzadeh M (2007): Destructive effects of the 2003 Bam earthquake on structures, *Asian Journal of Civil Engineering* (Building and Housing), **8** (3), 329-342.